Cell Biology:

Novel Role for Proteinase-activated Receptor 2 (PAR_2) in Membrane Trafficking of Proteinase-activated Receptor 4 (PAR_4)

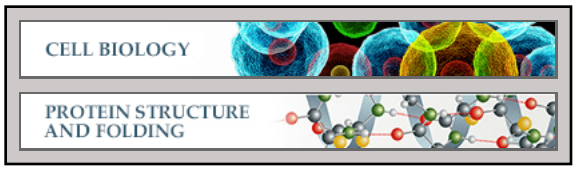

Margaret R. Cunningham, Kathryn A. McIntosh, John D. Pediani, Joris Robben, Alexandra E. Cooke, Mary Nilsson, Gwyn W. Gould, Stuart Mundell, Graeme Milligan and Robin Plevin

J. Biol. Chem. 2012, 287:16656-16669.
doi: 10.1074/jbc.M111.315911 originally published online March 12, 2012

⌘ *Author's Choice*

THE JOURNAL OF BIOLOGICAL CHEMISTRY VOL. 287, NO. 20, pp. 16656–16669, May 11, 2012

Novel Role for Proteinase-activated Receptor 2 (PAR_2) in Membrane Trafficking of Proteinase-activated Receptor 4 (PAR_4)*[S]

Received for publication, October 21, 2011, and in revised form, March 2, 2012 Published, JBC Papers in Press, March 12, 2012, DOI 10.1074/jbc.M111.315911

Margaret R. Cunningham[‡§1], Kathryn A. McIntosh[‡], John D. Pediani[¶], Joris Robben[¶‖], Alexandra E. Cooke[§], Mary Nilsson[‡], Gwyn W. Gould[**], Stuart Mundell[§], Graeme Milligan[¶], and Robin Plevin[‡]

*From the [‡]Department of Physiology and Pharmacology, Strathclyde Institute for Biomedical Sciences, Univesity of Strathclyde, 27 Taylor Street, Glasgow G4 0NR, Scotland, United Kingdom, the [¶]Molecular Pharmacology Group, Institute of Molecular, Cell and Systems Biology, College of Medical, Veterinary and Life Sciences, and **Henry Wellcome Laboratory of Cell Biology, Institute of Molecular, Cell and Systems Biology, College of Medical, Veterinary and Life Sciences, University of Glasgow, Glasgow G12 8QQ, Scotland, United Kingdom, the [‖]Department of Physiology, Nijmegen Centre for Molecular Life Sciences, Radboud University Nijmegen Medical Centre, Nijmegen, Netherlands, and the [§]School of Physiology and Pharmacology, University of Bristol, Bristol BS8 1TD, United Kingdom*

Background: Bioinformatic analysis revealed that PAR_4 possesses an ER retention motif.
Results: PAR_2 both abrogates and facilitates chaperone protein interaction with PAR_4 to allow PAR_4 to evade ER retention and be delivered to the plasma membrane.
Conclusion: PAR_2 regulates PAR_4 localization and cell signaling through heterodimerization.
Significance: Impact upon understanding PAR_2 and PAR_4 in inflammation where clear roles are defined.

Proteinase-activated receptors 4 (PAR_4) is a class A G protein-coupled receptor (GPCR) recognized through the ability of serine proteases such as thrombin and trypsin to mediate receptor activation. Due to the irreversible nature of activation, a fresh supply of receptor is required to be mobilized to the cell surface for responsiveness to agonist to be sustained. Unlike other PAR subtypes, the mechanisms regulating receptor trafficking of PAR_4 remain unknown. Here, we report novel features of the intracellular trafficking of PAR_4 to the plasma membrane. PAR_4 was poorly expressed at the plasma membrane and largely retained in the endoplasmic reticulum (ER) in a complex with the COPI protein subunit β-COP1. Analysis of the PAR_4 protein sequence identified an arginine-based (RXR) ER retention sequence located within intracellular loop-2 ($R^{183}AR \rightarrow A^{183}AA$), mutation of which allowed efficient membrane delivery of PAR_4. Interestingly, co-expression with PAR_2 facilitated plasma membrane delivery of PAR_4, an effect produced through disruption of β-COP1 binding and facilitation of interaction with the chaperone protein 14-3-3ζ. Intermolecular FRET studies confirmed heterodimerization between PAR_2 and PAR_4. PAR_2 also enhanced glycosylation of PAR_4 and activation of PAR_4 signaling. Our results identify a novel regulatory role for PAR_2 in the anterograde traffic of PAR_4. PAR_2 was shown to both facilitate and abrogate protein interactions with PAR_4, impacting upon receptor localization and cell signal transduction. This work is likely to impact markedly upon the understanding of the receptor pharmacology of PAR_4 in normal physiology and disease.

Proteinase-activated receptors (PARs)[2] are a class A GPCR family comprised of four family members, PAR_1 through to PAR_4, which play key roles in aspects of both physiology and pathophysiology including platelet aggregation, wound healing, and various aspects of inflammation (1–3). Detailed characterization of the protein structure of the PAR family has identified proteolytic cleavage sites at the receptor N-terminal (4–7). For each receptor a unique tethered ligand is exposed within the N-terminal that interacts with the second extracellular loop to mediate receptor activation. The structural determinants that regulate PAR activation have long been of interest and there has been considerable focus placed upon the mechanisms underpinning membrane trafficking and signal termination particularly for PAR_1 (8–14) and PAR_2 (15–19). The most recent family member to be cloned, PAR_4 (20, 21), is distinct from both PAR_1 and PAR_2. Although a thrombin-activated receptor, it lacks the hirudin-like domain required for thrombin selectivity and is activated by several other ligands including trypsin. In addition it has a shorter C terminus than PAR_1 and PAR_2 and lacks essential phosphorylation sites within intracellular domains, which are present in other family members and have been shown to be necessary for receptor desensitization (22). PAR_4 has been poorly studied relative to either PAR_1 or PAR_2 but has been shown to signal via Ca^{2+} mobilization and to

* This work was supported in part by Wellcome Trust Grant 08444/Z/09/Z (to R. P.), British Heart Foundation Grant BHF-FS/05/014 (to R. P.), and Medical Research Council Grant G0900050 (to G. M.).
⌘ *Author's Choice*—Final version full access.
[S] This article contains supplemental Figs. S1–S3.
[1] Recipient of the 2006 British Pharmacological Society AJ Clark Ph.D. Student award. To whom correspondence should be addressed: School of Physiology and Pharmacology, Medical Sciences Building, University of Bristol, Bristol BS8 1TD, United Kingdom. Tel.: 44-01173311433; E-mail: margaret.cunningham@bristol.ac.uk.

[2] The abbreviations used are: PAR, proteinase-activated receptor; ER, endoplasmic reticulum; GPCR, G protein-coupled receptor; mEGFP/mEYFP/mECFP, monomeric enhanced green/yellow/cyan fluorescent protein; RXR, arginine-based ER retention motifs; COPI, coat protein I complex; RFRET, ratiometric FRET.

regulate the MAP kinases (23). However, very little is known of the mechanisms regulating receptor trafficking.

Due to the irreversible nature of activation of PARs, for responsiveness to agonist to be retained, fresh supplies of receptor are required to be mobilized to the cell surface. Delivery to the membrane requires efficient transport between the ER/Golgi/plasma membrane, which can be facilitated through discrete motifs that reside within the synthesized protein (24, 25). Many chaperone proteins, such as coat protein complexes (COPI and COPII), can assist transport of recently synthesized proteins through motif-based sorting (26–28). Properly assembled proteins are packaged for export into COPII vesicles where they progress to the ER-Golgi intermediate complex, a process known as anterograde transport. Misfolded proteins or those exposing sequences encoding ER retention motifs (for example, RXR, KDEL, or KKAA motifs) are shuttled back to the ER via COPI vesicles, in a process known as retrograde transport (29). During the assembly of multimeric proteins, such as GPCR homo/heterodimers, proteins possessing ER retention signals have been shown to evade ER retention through the steric masking of motifs during protein folding (30–33). 14-3-3 proteins have previously been shown to assist motif masking to ensure export of proteins to the Golgi (25, 34). Once proper protein folding has been achieved, post-translational modifications, such as complex glycosylation, will occur (35).

Here we identify for the first time the presence of an arginine-based ER retention motif within intracellular loop-2 of PAR_4, which results in ER retention through COPI-dependent retrograde transport. In the presence of PAR_2, through PAR_2/PAR_4 heterodimer formation and interaction with 14-3-3ζ, PAR_4 was able to evade ER retention and undergo *N*-linked complex glycosylation. This resulted in efficient delivery to the plasma membrane. The impact of enhanced cell surface expression was reflected in enhanced PAR_4-mediated cell signal transduction. PAR_2 is often co-expressed with PAR_4, and they are dual up-regulated by various pro-inflammatory mediators and have been shown to be co-activated by common agonists (20, 36, 37). In the presence of PAR_2, a significant increase in PAR_4-mediated total inositol phosphate accumulation was observed. This work demonstrates for the first time a novel regulatory role for PAR_2 in the anterograde traffic and signaling of PAR_4. This is mediated by selective interaction with COPI or 14-3-3 proteins, offering a new paradigm for class A GPCR trafficking and control.

EXPERIMENTAL PROCEDURES

Reagents and Antibodies—The PAR_4 activating peptide, Ala-Tyr-Pro-Gly-Lys-Phe-amidated (NH_2) peptide (AYPGKF-NH_2), was synthesized by the University of Calgary Peptide Service (Calgary, Canada). ER-Tracker^{TM} Blue-White DPX Dyes (Molecular Probes) for ER labeling and the anti-transferrin receptor mouse monoclonal antibody were purchased from Invitrogen Ltd. Rabbit polyclonal anti-Na^+,K^+-ATPase α1 antibody was purchased from Cell Signaling Technology Inc. Living Colors® full-length A.v. GFP rabbit polyclonal antibody was purchased from Clontech-TaKaRa Bio Europe (France). PKH26 Red Fluorescent Cell Linker kit for general cell membrane labeling, anti-PAR_4 goat polyclonal, anti-14-3-3ζ rabbit polyclonal antibodies, monoclonal anti-HA-agarose conjugate, HA peptide, and tunicamycin were from Sigma. The anti-PAR_4 rabbit polyclonal antibody was obtained from Abcam (Cambridge, UK). Anti-β coatomer protein (β-COP1) rabbit polyclonal antibody was purchased from Pierce and Thermo Fisher Scientific (Loughborough, UK). Mouse monoclonal anti-HA antibody was purchased from Cambridge Bioscience (Cambs, UK). Pierce Cell Surface Protein Isolation Kit was purchased from Thermo Scientific. The alkaline phosphatase substrate kit was obtained from Bio-Rad.

Epitope-tagged PAR Constructs—Human PAR_2 was amplified by polymerase chain reaction (PCR) from a pRSV-PAR_2 vector.

The PCR product was then digested with HindIII-BamHI and cloned into the respective sites of a pEYFP-N1 vector (Clontech). Human PAR_4 was amplified from a pcDNA3.1(+)-hPAR_4 vector by PCR and digested with Kpn-AgeI, whereas ECFP was amplified from the pECFP-N1 vector (Clontech) and digested with AgeI-XbaI. PAR_4 and ECFP were ligated and cloned into the KpnI-XbaI sites of the pcDNA3.1(+) vector. Monomeric ECFP and EYFP constructs were generated by amino acid substitution of Ala^{206} to Lys^{206} (38), through site-directed mutagenesis using the Gene Tailor^{TM} Site-directed Mutagenesis System (Invitrogen). Amino acid substitutions were similarly made within the primary sequence of PAR_4 to mutate potential arginine-based ER retention motifs (positions $R^{183}AR \rightarrow A^{183}AA$, (referred to as RAR mut) $R^{188}GRR \rightarrow A^{188}GAA$ and $R^{183}AR$ $R^{188}GRR \rightarrow A^{183}AA$ $A^{188}GAA$) and the *N*-linked glycosylation site on the N-terminal of PAR_4 ($Asn^{56} \rightarrow Ala^{56}$). A HA epitope tag (YPYDVPDYA) was incorporated into the C-terminal of PAR_4 by PCR to generate PAR_4-HA. All constructs were confirmed by sequencing.

Cell Culture—HEK293 cells were maintained in minimal essential medium with Earle's salts, L-glutamine supplemented with 10% fetal calf serum (FCS), penicillin (100 units ml^{-1}), streptomycin (100 $\mu g\ ml^{-1}$), and nonessential amino acids and passaged using 1× SSC (sodium citrate, pH 7.4). NCTC-2544 cells and NCTC-PAR_2 cells were grown in Medium 199 with Earle's salts (Sigma) containing 10% FCS, sodium bicarbonate (50 mM), L-glutamine (2 mM), penicillin (100 units ml^{-1}), and streptomycin (100 $\mu g\ ml^{-1}$). NCTC-2544 cells were passaged using Versene (0.53 mM EDTA in PBS) to avoid trypsin exposure. All cells where then incubated at 37 °C in a humidified atmosphere with 5% CO_2 with medium replaced every 2 days.

Transient Transfection—Cells were grown in 12- and 6-well plates or T75 flasks prior to transient transfection at 70–80% confluence with 1, 2, or 10 μg of endo-free plasmid DNA, respectively, using Lipofectamine 2000 (Invitrogen) following the recommended manufacturer's guidelines. Maximal gene expression was observed 48 h post-transfection.

Inositol Phosphate Accumulation Assay—Following transient transfection for 24 h, cells were serum starved for a further 24 h in serum-free medium supplemented with 0.5 μCi/well (1 Ci = 37 GBq) of *myo*-[2-^{3}H]inositol (PerkinElmer Life Sciences) (0.5 μCi/well; 1 Ci = 37 GBq). Cells were pretreated with 20 mM lithium chloride for 30 min prior to agonist treatment (100 μM AYPGKF-NH_2 for 45 min). Measurement of the accumulation of inositol phosphates was carried out as previously described by Plevin *et al.* (39).

Fluorescence Microscopy—Cells were washed in PBS prior to methanol fixation for 15 min at room temperature. After further washes with PBS, cells were stained using 4′,6-diamidino-2-phenylindole (DAPI) nuclear dye or ER Tracker™ dye then mounted onto glass microscope slides with 15 μl of mowiol (Calbiochem). Cells were visualized using a Nikon TE300-E microscope (Nikon Instruments, New York) using a ×100 (numerical aperture; NA 1.3) oil immersion Fluor lens. Emitted fluorescence was detected using a photometric Cool Snap-HQ monochrome camera (Roper Scientific, Trenton, NJ) set up in 12-bit mode (0–4095 gray tones). Metamorph software (version 7.0, Molecular Devices Corp., Downing, PA) was used to control image acquisition and modify image settings. Images were background corrected, based on statistical correction of average background regions from defined regions of interest.

Cell Surface ELISA—Changes in cell surface expression of PAR$_4$ were measured by Enzyme-linked ImmunoSorbent Assay (ELISA). Cells were transfected with PAR$_4$ for 24 h prior to being seeded at a density of 1×10^5 cells per well in 24-well plates pre-coated with 0.1 ml/ml of poly-L-lysine. Cells were grown overnight to recover. Surface receptors were pre-labeled with anti-PAR$_4$ (1/1000 dilution) at 4 °C for 1 h. Cells were fixed in 3.7% paraformaldehyde for 5 min and then washed three times in Tris-buffered saline (TBS; 20 mM Tris, pH 7.5, 150 mM NaCl). Cells were blocked with 1% BSA in TBS for 45 min at room temperature followed by a 1-h inculation with a alkaline phosphatase-conjugated goat anti-rabbit antibody (1/1000 dilution) in 1% BSA in TBS. Cells were washed four times in TBS to remove unbound secondary antibody. Alkaline phosphate substrate solution was prepared by dissolving *p*-nitrophenyl phosphate tablets in diethanolamine buffer (Bio-Rad). Substrate solution was added to cells and the plates were incubated at 37 °C for 10–30 min. Absorbance was measured at 405 nm using a microplate reader (Dynex MRX revelation).

Cell Surface Biotinylation—Surface expression of PAR$_4$ in NCTC-2544 and NCTC-PAR$_2$ cells was measured by a biotinylation assay using Pierce Cell Surface Protein Isolation Kit (Thermo Scientific). Briefly, four T75 cm^2 flasks of NCTC-2544 or NCTC-PAR$_2$ cells were transfected with PAR$_4$ mECFP. Cells were labeled with Sulfo-NHS-SS-Biotin for 30 min at 4 °C on a rocking platform. The biotinylation reaction was stopped through the addition of a quench solution followed by further incubation at 4 °C for 15 min. Cells were scraped and the flasks were rinsed in Tris-buffered saline (TBS) and centrifuged at 1,000 × *g* for 3 min. Supernatant was discarded and the cell pellets were washed 3 times in TBS followed by centrifugation at 1,000 × *g* for 3 min. Cells were lysed using the provided lysis buffer containing complete protease inhibitor mixture (Roche Diagnostics) and sonicated on ice at low power to disrupt using five 1-s bursts, then incubated at 4 °C for 30 min on an orbital rotator. The cell lysates were then centrifuged at 10,000 × *g* for 2 min at 4 °C. Clarified supernatants were transferred to a new tube and incubated with NeutrAvidin-agarose for 60 min at room temperature with end-over-end mixing using a rotator. Supernatant/agarose slurry was centrifuged for 1 min at 1,000 × *g* and the supernatant was discarded. The agarose pellet was washed 3 times in the wash buffer provided with the addition of complete protease inhibitor mixture. SDS-PAGE sample buffer (62.5 mM Tris-HCl, pH 6.8, 1% SDS, 10% glycerol, 50 mM DTT) was added to the sample, which was then heated in a heat block for 5 min at 95 °C. The tubes were then centrifuged for 2 min at 1,000 × *g*. PAR$_4$ expression was detected by Western blotting using antibodies specific for either PAR$_4$ or GFP. Equal expression of total levels of PAR$_4$ mECFP in transfected cells was confirmed by resolving the corresponding whole cell lysates prepared from the same cells used for the biotinylation experiments.

Western Blotting—Proteins were separated by 8–10% SDS-PAGE and transferred onto nitrocellulose membrane. The membranes were blocked for nonspecific binding in 2% BSA (w/v) diluted in NATT buffer (50 mM Tris-HCl, 150 mM NaCl, 0.2% (v/v) Tween 20) for 2 h. The blots were then incubated overnight with 50 ng/ml of primary antibody diluted in 0.2% BSA (w/v) in NATT buffer then washed with NATT buffer at 15-min intervals for a further 90 min. The blots were then incubated with HRP-conjugated secondary antibody (20 ng/ml) in 0.2% BSA (w/v) diluted in NATT buffer for 2 h. After a further 90-min wash, the membranes were treated with ECL reagent and exposed to Kodak x-ray film.

Subcellular Fractionation of ER and Plasma Membrane Compartments—Cells were grown to 70–80% confluence in 5 × T150 cm tissue culture flasks prior to transient transfection with PAR$_4$ mECFP. The cells were harvested and the cell pellet resuspended in 3 ml of HES buffer (25 mM HEPES, 1 mM EDTA, and 250 mM sucrose, pH 7.4) supplemented with protease inhibitors (25 μg/ml of leupeptin, 10 μg/ml of aprotinin, and 1 μg/ml of PMSF). The cell lysate was homogenized using a pre-cooled cell homogenizer (Isobiotec Precision Engineering, Germany, German Patent Office number 202 09 547.9) fitted with a size 10-μm clearance tungsten carbide ballbearing. The homogenate was centrifuged at 500 × *g* for 2 min at 4 °C and the supernatant was transferred to a fresh tube and resuspended in Opti-prep (Invitrogen) density gradient medium to create a 45% (v/v) density sample solution. A density gradient (30–10%) was prepared using Opti-prep medium mixed in HES buffer followed by ultracentrifugation at 72,000 × *g* for 4 h at 4 °C to separate plasma membrane, endosomal, and ER fractions (40). Equal volume fractions (300 μl) were collected and precipitated in 37.5% TCA, incubated on ice for 15 min, and centrifuged at 14,000 × *g* for 15 min at 4 °C. The cell pellets obtained were resuspended in 2× Laemmli sample buffer supplemented with 1 M urea and resolved by Western blotting. Subcellular fractionation of ER and plasma membrane compartments were determined using Na^+,K^+-ATPase, transferrin receptor, and calnexin antibodies as markers for plasma membrane, endosomal, and ER fractions, respectively.

Intermolecular FRET—Wide-field intermolecular FRET microscopy was performed at room temperature in living cells (41–43) on a Nikon TE2000-E inverted microscope (Nikon Instruments, Melville, NY). Cells were grown on 0 thickness on coverslips and transiently transfected with the appropriate monomeric donor mECFP or acceptor mEYFP-tagged constructs. Coverslips were placed into a microscope chamber containing physiological HEPES-buffered saline solution (130 mM NaCl, 5 mM KCl, 1 mM $CaCl_2$, 1 mM $MgCl_2$, 20 mM HEPES, 10 mM D-glucose, pH 7.4). FRET imaging was performed using

a ×40 (numerical aperture; NA 1.3) oil immersion Fluor lens. Emitted fluorescence was detected using a photometric Cool Snap-HQ monochrome camera (Roper Scientific, Trenton, NJ) set up in 12-bit mode (0–4095 gray tones). MetaMorph software (version 7.6.4 Molecular Devices Corp.) was used to control both the microscopy hardware and multiwavelength fluorescence image acquisition required for intermolecular FRET detection. Donor 430 nm or acceptor 500 nm excitation light was generated using a computer controlled Optoscan monochromator (Cairn Research, Faversham, Kent, UK) coupled to a 103/W2 mercury (Hg) arc lamp source (Cairn Research). Optimization of illumination excitation center wavelength and band pass settings was performed to prevent cross-excitation, minimize donor and acceptor bleed-through into the FRET channel, and ensure no recorded pixels within the channel images were saturated above a gray level intensity value of 4095. The risk of motion occurring during the sequential FRET imaging process was minimized by using a high-speed filter wheel (Prior Scientific Instruments, Cambridge, UK). Metamorph imaging software was used to quantify the FRET images using the specified bleed-through FRET method. Corrected FRET (FRETc) was calculated using a pixel-by-pixel methodology using the equation FRETc = FRET − (coefficient B × mECFP) − (coefficient A × mEYFP), where mECFP, mEYFP, and FRET values correspond to background corrected images obtained through the donor mECFP, mEYFP, and FRET channels. B and A correspond to the values obtained for the mECFP (donor) and mEYFP (acceptor) bleed-through coefficients, respectively, calculated using cells transfected with either the mECFP or mEYFP protein alone. Ratiometric FRET (RFRET) values were calculated from the measurements taken from raw FRET fluorescence and dividing this value by the total spectral bleed-through of the acceptor and donor into the FRET channel, *i.e.* raw FRET divided by (acceptor multiplied by **(a)**) + (donor multiplied by **(b)**). In the absence of energy transfer (*i.e.* no FRET occurrence), the RFRET value measured is ~1, values greater than 1 represent the occurrence of FRET, thus indicative of protein interaction.

Co-immunoprecipitation—To measure PAR_4 interaction with 14-3-3ζ, cells transiently expressing PAR_4-HA were washed with PBS prior to solubilization in lysis buffer (20 mM HEPES buffer, pH 7.7, containing 50 mM NaCl, 0.1 mM EDTA, 0.1 mM Na_3VO_4, 0.1 mM PMSF, 10 mg/ml of aprotinin, 10 mg/ml of leupeptin, and 1% (w/v) Triton X-100). After a 1-h rotation at 4 °C, the cell lysates were clarified by centrifugation at 13,000 × *g* for 5 min at 4 °C. Supernatants were transferred to fresh Eppendorf tubes and 50 μl was removed for inputs. The remaining lysate was pre-cleared with 30 μl of protein G/protein A-agarose (Calbiochem) and placed in an rotator for 1 h at 4 °C. Samples were centrifuged at 4 °C for 5 min at 5,000 × *g* and the pre-cleared lysate was transferred to fresh Eppendorf tubes containing 30 μl of monoclonal anti-HA-agarose conjugate (Sigma) and rotated overnight at 4 °C. Samples were centrifuged at 4 °C for 5 min at 5,000 × *g*, then washed with 500 μl of lysis buffer three times and proteins were eluted by incubation with 30 μl of anti-HA peptide (Sigma; 200 μg/ml) for 10 min at room temperature. Eluted proteins were removed and added to 10 μl of 5× SDS sample buffer and boiled at 95 °C for 10 min prior to SDS-PAGE.

Statistical Analysis—Where experimental data are shown as a blot, this represents one of at least 3 experiments and data represent the mean ± S.E. Statistical analysis was by one-way analysis of variance with Dunnett's post-test (*, $p < 0.05$; **, $p < 0.01$).

RESULTS

Intracellular Retention of PAR_4 in the Endoplasmic Reticulum—To monitor the expression level and localization of PAR_4, the receptor was tagged at the C terminus with a monomeric variant form of enhanced cyan fluorescent protein (mECFP) and transiently expressed in keratinocyte-derived NCTC-2544 cells. These cells provided an ideal model for these investigations, due to the lack of endogenous PAR expression (44). The localization of PAR_4 was initially monitored using fluorescence microscopy of NCTC-2544 cells transiently expressing PAR_4 mECFP (Fig. 1*A*). In comparison to cells expressing either PAR_1 mEYFP or PAR_2 mEYFP, PAR_4 mECFP was largely retained inside the cell with only weak membrane localization observed. Further microscopy in cells treated with an ER tracker dye (Fig. 1*B*) highlighted that PAR_4 mECFP was predominantly retained in the ER.

Presence of a Functional Arginine-based ER Retention Motif within PAR_4—Analysis of the protein sequence for PAR_4 identified two potential arginine-based (RXR) ER retention motifs located within the intracellular loop-2 of the receptor (supplemental Fig. S1). Alignment of the primary sequences for all PAR family members found that these motifs were unique to PAR_4. The contribution of these motifs in controlling the cellular localization of PAR_4 was assessed by removing the arginine residues by alanine substitution (RXR → AXA). Of the possible motifs investigated, only mutation of the R^{183}AR to A^{183}AA resulted in a loss of ER retention and allowed PAR_4 to translocate to the plasma membrane (Fig. 2*A*). Receptor expression levels were determined by Western blotting (Fig. 2*B*). Following expression of PAR_4 mECFP the appearance of a protein band, resolving around 65 kDa, was observed. This corresponded well with the predicted molecular mass of PAR_4 mECFP (38 kDa for PAR_4 combined with 27 kDa for the mECFP). As Fig. 2*B* shows, as the expression of the R^{183}AR mutant increased, the appearance of multiple protein forms was observed, a doublet resolving around 65 kDa and a slightly larger species resolving between 70 and 80 kDa. Subcellular fractionation of cells expressing either PAR_4 mECFP or the R^{183}AR mutant was carried out to separate plasma membrane, endosomal, and ER compartments followed by Western blot (Fig. 2*C*). The 65-kDa protein species observed in cells expressing PAR_4 mECFP or mutant receptor reached maximal levels in ER and endosomal fractions (*lanes 4–7*), co-locating with calnexin and transferrin markers, respectively. These experiments identified that the higher molecular mass species observed in cells expressing the R^{183}AR mutant reflected receptors located in the plasma membrane and endosome compartments (*lanes 1–4*) as shown using Na^+,K^+-ATPase and transferrin receptor markers, respectively.

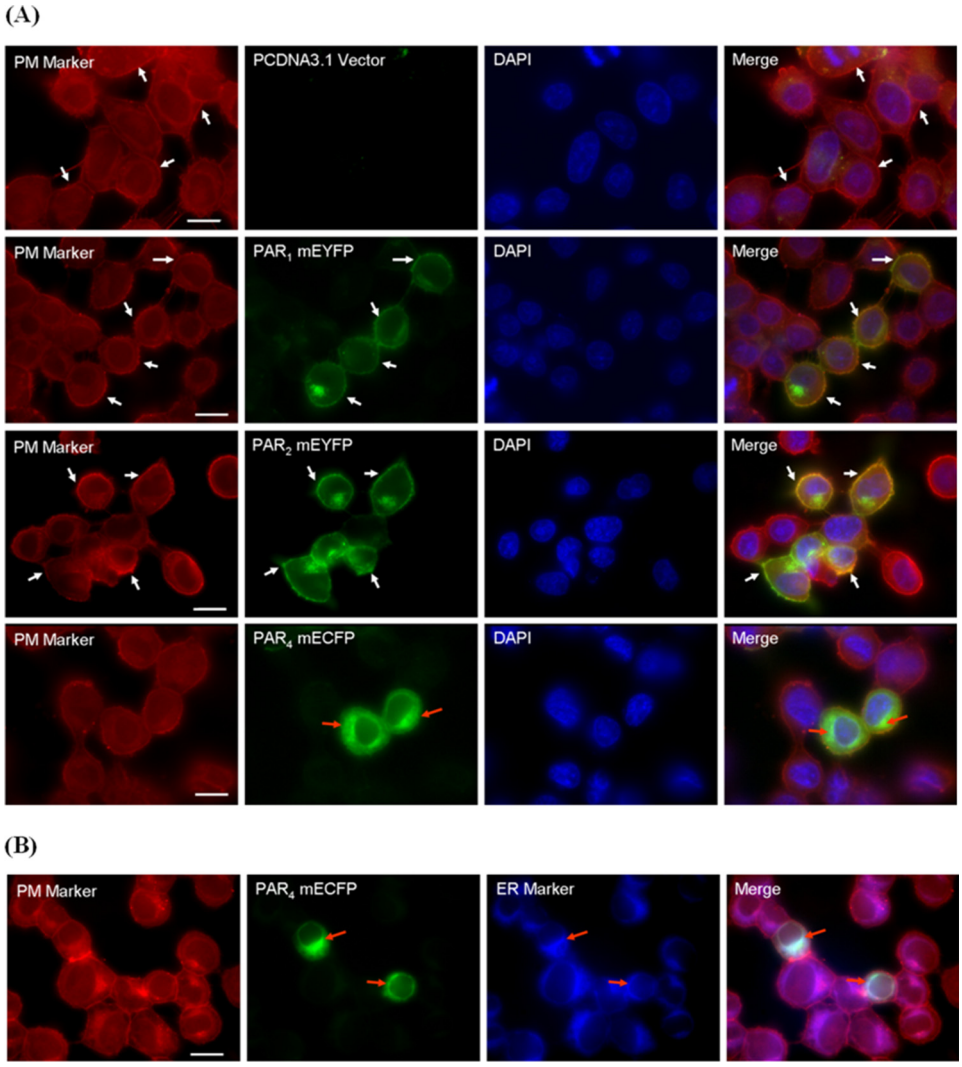

FIGURE 1. **Retention of PAR$_4$ in the ER.** NCTC-2544 cells expressing pcDNA3.1 empty vector, PAR$_1$ mEYFP, PAR$_2$ mEYFP, or PAR$_4$ mECFP (*green*) were treated with PKH26 red fluorescent cell linker dye to stain the plasma membrane (*PM*, *red*). Cells were fixed and treated with either (*A*) 4′,6-diamidino-2-phenylindole (*DAPI*) to identify nuclei (*blue*) or (*B*) ER marker (ER-Tracker Blue-White DPX Dyes, Molecular Probes) to identify the ER (*blue*). Cells were visualized using a ×100 Plan Fluor objective. Images were merged to highlight distinct plasma membrane, nucleus, or ER compartments. *Scale bars* = 10 μm. *White arrows* point to the plasma membrane, whereas *red arrows* are indicative of the intracellular/ER compartmentalization of PAR$_4$. Image set representative of three separate experiments.

Coat protein I complex (COPI) can target proteins for retention through recognition and interaction with RXR motifs (29). COPI is comprised of multiple subunits including α-, β-, β′-, γ-, δ-, ϵ-, and ζ-COP. The ability of COPI to interact with PAR$_4$ was demonstrated through co-immunoprecipitation with the β-COP subunit of the COPI complex as shown in Fig. 2*D*.

PAR$_2$ Facilitates Anterograde Transport of PAR$_4$ and Interaction with 14-3-3ζ—The presence of the R^{183}AR ER motif in the protein sequence contributed greatly to the retention of PAR$_4$ in the ER. Despite the presence of this ER retention motif, as the earlier original characterization studies show, PAR$_4$ has the ability to reach the plasma membrane and respond to protease activation (20). During the assembly of multimeric proteins it has been shown that ER motifs, particularly arginine-based ER retention motifs (25), may be masked to allow proteins to evade the quality control processes in the ER (31, 45). Interestingly when co-expressed with PAR$_2$ mEYFP, PAR$_4$ mECFP was found to be localized at the plasma membrane with minimal intracellular compartmentalization, as shown by confocal microscopy in Fig. 3*A*. This was explored further by cell surface ELISA using an N-terminal PAR$_4$-specific antibody to quantify differences in surface receptor levels in NCTC-2544 cells and NCTC-2544 cells stably expressing PAR$_2$ (NCTC-PAR$_2$), as shown in Fig. 3*B*. When PAR$_4$ mECFP was expressed in NCTC-2544 cells a small increase in absorbance (A405 nm) was detected (0.676 ± 0.05, *, $p \leq 0.05$, $n = 4$) compared with control untransfected cells (0.495 ± 0.05, $n = 4$). When expressed in NCTC-PAR$_2$ cells, PAR$_4$ surface expression was significantly increased, as demonstrated by the enhanced $A_{405\ nm}$ reading (1.016 ± 0.03, N4, ***, $p \leq 0.001$ compared with PAR$_4$ in NCTC-2544 cells). Enhanced translocation of PAR$_4$ mECFP to the plasma membrane was not replicated when co-expressed with PAR$_1$ mEYFP (supplemental Fig. S2). PAR$_4$ was still largely localized intracellularly, with PAR$_1$/PAR$_4$ co-localization observed predominantly within vesicles.

As shown in Fig. 4*A*, similar membrane translocation was observed for PAR$_4$ mECFP when transfected into NCTC-PAR$_2$.

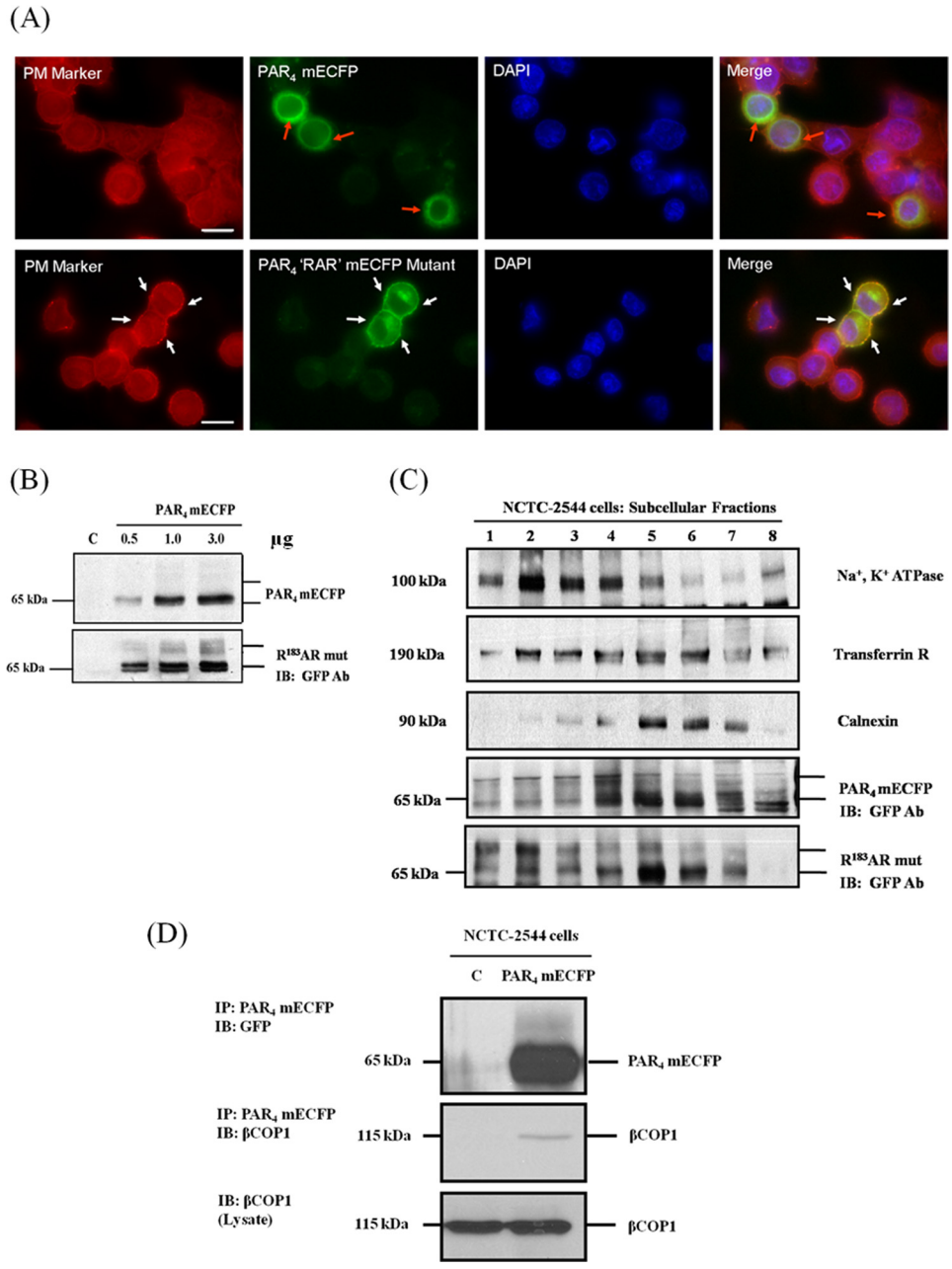

FIGURE 2. **Mutation of the arginine-based ER retention motif (R^{183}AR) enhances the cell surface expression of PAR$_4$.** *A*, NCTC-2544 cells expressing PAR$_4$ mECFP or PAR$_4$ RAR mECFP mutant (*green*) were treated to stain for the plasma membrane (*PM*, *red*) and nucleus (*blue*) as previously described. Cells were visualized using a ×100 Plan Fluor objective. *Scale bars* = 10 μm. Intracellular retention of PAR$_4$ mECFP is highlighted (*red arrows*), whereas notable membrane localization of the PAR$_4$ RAR mECFP is evident (*white arrows*). *B,* protein expression was assessed using Western blotting of whole cell lysates expressing increasing amounts of PAR$_4$ mECFP or PAR$_4$ RAR mECFP constructs as indicated. *C,* changes in the surface expression of PAR$_4$ were confirmed by subcellular fractionation using differential ultracentrifugation on an iodixanol gradient in cells expressing PAR$_4$ mECFP or PAR$_4$ RAR mECFP. Fractions were precipitated and resolved by SDS-PAGE followed by Western blotting. PAR$_4$ mECFP (predicted band size ~65 kDa) was detected using a polyclonal GFP antibody capable of recognizing the ECFP at the C-terminal of PAR$_4$. Na^+,K^+-ATPase (~100 kDa), transferrin receptor (~190 kDa), and calnexin (90 ~kDa) antibodies were used for the detection of membrane, endosomal, and ER compartments, respectively. *D*, interaction between PAR$_4$ and COPI complex proteins was confirmed by co-immunoprecipitation. Lysates from NCTC-2544 cells expressing PAR$_4$ mECFP were subjected to immunoprecipitation (*IP*) and then probed for β-COP1 interaction. Images and blots are representative of three separate experiments.

In addition, when PAR$_4$ mECFP was resolved by Western blotting two clear protein forms were detected when expressed in NCTC-PAR$_2$ cells (Fig. 4*B*). These results were similar to the observations made in previous experiments resolving the ER retention motif mutant PAR$_4$ protein. Subsequent subcellular fractionation of NCTC-PAR$_2$ cells expressing PAR$_4$ mECFP highlighted the distinct differences in the compartmentalization of PAR$_4$. As Fig. 4*B* shows, the more rapidly migrating 65-kDa species was confined to ER and endosomal compartments (*lanes 4–6*), whereas the distribution of the less rapidly migrating form strongly correlated with ER, endosomal, and plasma membrane fractions (*lanes 1–6*). Enhanced surface expression of PAR$_4$ was subsequently quantified using cell surface biotinylation, as shown in Fig. 4*C*. Following biotinylation of surface proteins, expression of PAR$_4$ was probed using both anti-GFP and anti-PAR$_4$ specific antibodies in NCTC-2544 and

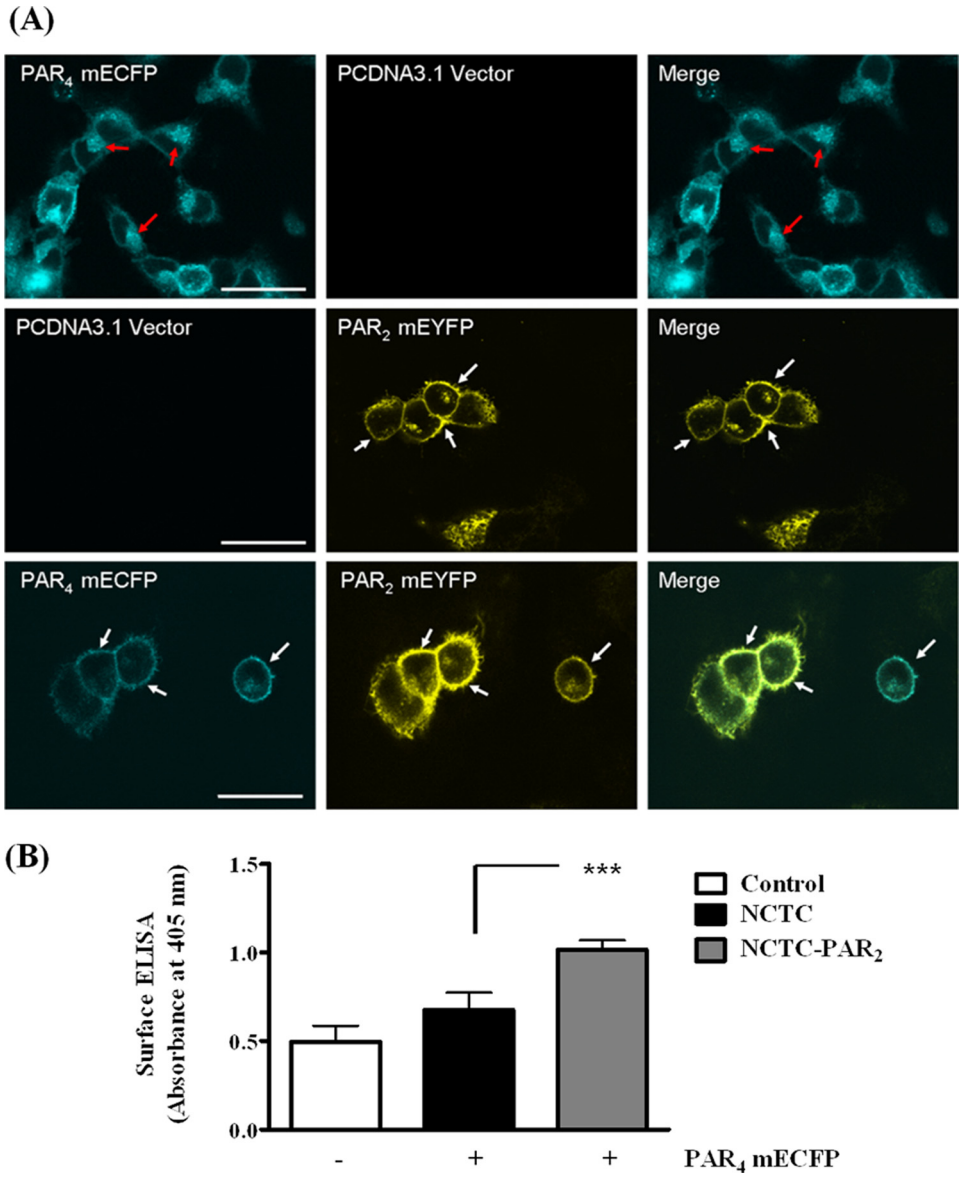

FIGURE 3. **PAR$_2$ enhances surface expression of PAR$_4$ when co-expressed in NCTC-2544 cells.** NCTC-2544 cells expressing PAR$_4$ mECFP (*cyan*), PAR$_2$ mEYFP (*yellow*), or co-expressing both constructs were fixed for confocal microscopy. *Scale bars* = 25 μm. *A*, membrane (*white arrows*) receptor expression is highlighted, whereas intracellular receptor pools are indicated using *red arrows*. Images shown are representative of at least five independent experiments. *B*, enhancement of PAR$_4$ surface expression in the presence of PAR$_2$ was subsequently quantified using a surface ELISA approach with an N-terminal anti-PAR$_4$ antibody to detect changes in surface levels of PAR$_4$. Data are presented as the optical density at 405 nm obtained from NCTC-2544 cells only (*Control*), NCTC-2544 or NCTC-PAR$_4$ cells expressing PAR$_4$ mECFP performed in at least three independent experiments. ***, $p = 0.001$ one-way analysis of variance with Dunnett's post-test.

NCTC-PAR$_2$ cells transfected with PAR$_4$ mECFP. Although detection of surface PAR$_4$ was negligible in transfected NCTC-2544 cells (0.725 ± 0.30-fold increase over mock transfected cells, $n = 4$), a significant increase in surface PAR$_4$ was detected in NCTC-PAR$_2$-transfected cells (5.199 ± 0.85-fold increase over mock cells, $n = 4$). In addition to enhanced cell surface expression of PAR$_4$ in the presence of PAR$_2$, a notable increase in the ability of PAR$_4$ to interact with the ζ isoform of the ER export chaperone 14-3-3 was detected in co-immunoprecipitation experiments (Fig. 4*D*). When PAR$_4$-HA was expressed in the parental NCTC-2544 cells, the ability of 14-3-3ζ to interact with PAR$_4$ was negligible. However, when PAR$_4$-HA was expressed in NCTC-PAR$_2$ cells, the ability of 14-3-3ζ to interact with PAR$_4$ was clearly shown. Differential interaction of PAR$_4$ with 14-3-3ζ was also demonstrated using GST pulldown assays employing GST-14-3-3ζ fusion proteins (supplemental Fig. S3). PAR$_4$ binding to GST-14-3-3ζ was enhanced when expressed in NCTC-PAR$_2$ cells. In addition, interaction between PAR$_4$ and β-COP1 was no longer observed during co-expression of PAR$_2$ and PAR$_4$ (Fig. 4*E* and supplemental Fig. S3).

The localization of PAR$_4$ was further explored in HEK293 cells, which have an endogenous level of PAR$_2$ (Fig. 5). When expressed, PAR$_4$ mECFP was observed both at the plasma membrane and in intracellular compartments (Fig. 5*A*), which when resolved by Western blot (Fig. 5*B*) identified similar protein species as in NCTC-2544 cells, representative receptor populations were expressed at the cell surface and in ER/endosomal compartments (Fig. 5*C*).

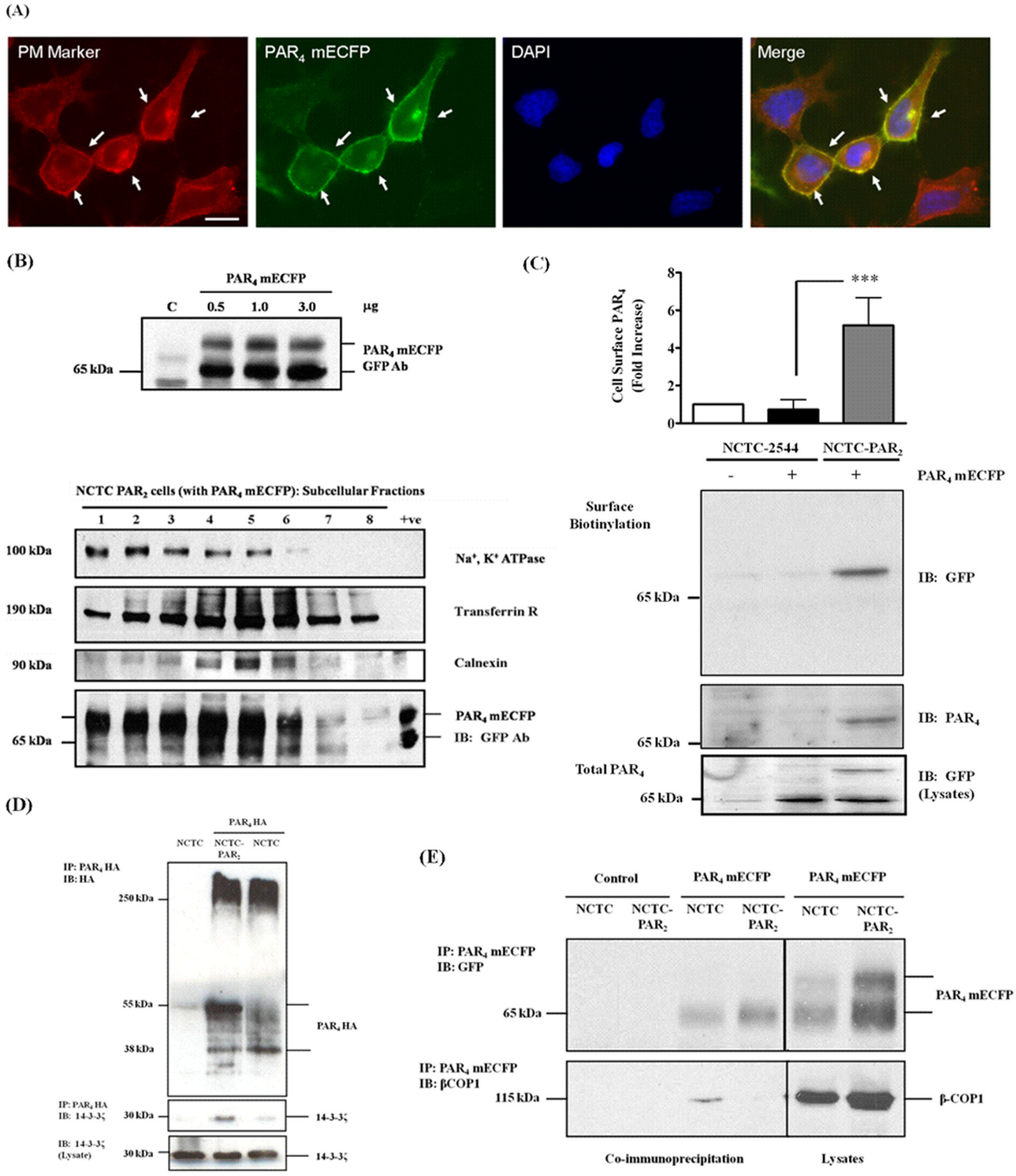

FIGURE 4. **PAR$_2$ facilitates interaction between PAR$_4$ and 14-3-3ζ but disrupts interaction with β-COP1.** PAR$_4$ mECFP was transiently transfected into NCTC overexpressing PAR$_2$ (NCTC-PAR$_2$) cells. *A*, cells were treated, as described previously, to identify the plasma membrane (*red*) and nuclei (*blue*). Cells were visualized using a ×100 Plan Fluor objective. Images were merged to highlight distinct plasma membrane/nuclear compartments. *Scale bars* = 10 μm. Enhanced surface expression of PAR$_4$ in NCTC-PAR$_2$ cells is indicated by *white arrows*. *B*, protein expression was assessed using Western blotting in cells expressing increasing amounts of PAR$_4$ mECFP with the protein bands were detected separated by subcellular fractionation in NCTC-PAR$_2$ cells and resolved by Western blotting, as previously shown. *C*, enhanced surface expression was then quantitatively assessed by cell surface biotinylation of NCTC-2544 and NCTC-PAR$_2$ cells expressing PAR$_4$ mECFP. Interaction between (*D*) PAR$_4$-HA and 14-3-3ζ or (*E*) PAR$_4$-mECFP and the βCOP subunit of COPI was assessed by co-immunoprecipitation (*IP*) in NCTC-2544 and NCTC-PAR$_2$ cells. Images and blots are representative of at least four independent experiments.

The novel features of PAR$_2$/PAR$_4$ co-expression were investigated further to identify if enhancement of the PAR$_4$ cell surface expression was a result of interaction between PAR$_2$ and PAR$_4$. For this purpose, wide field intermolecular FRET imaging was carried out (41, 42) in HEK293 cells expressing either PAR$_4$ mECFP or PAR$_2$ mEYFP alone or co-expressing these two

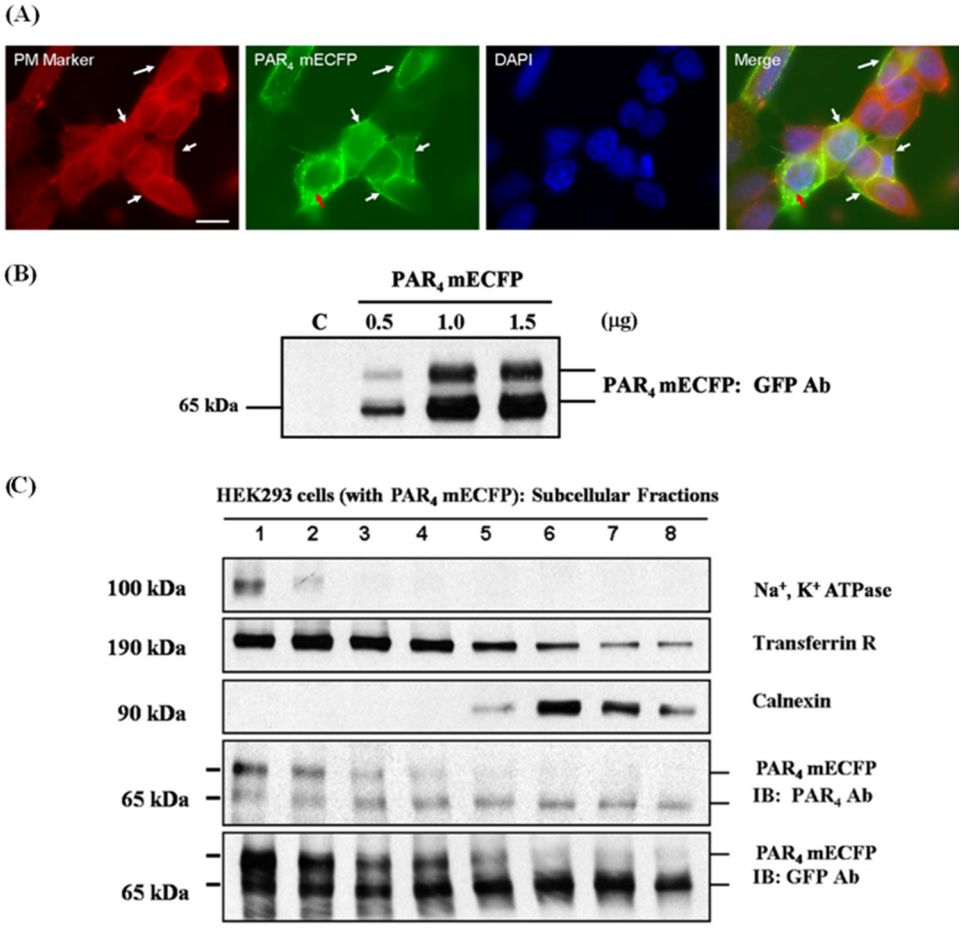

FIGURE 5. **Membrane localization of PAR$_4$ mECFP in HEK293 cells.** PAR$_4$ mECFP was transiently transfected into HEK293 cells that endogenously express PAR$_2$. *A*, localization of PAR$_4$ at the cells surface is shown by co-localization with a plasma membrane marker (*white arrows*). Cells were visualized using a ×100 Plan Fluor objective. *Scale bars* = 10 μm. *B*, the protein band pattern of PAR$_4$ expression was further assessed by Western blot of transfected whole cell lysates followed by subcellular fractionation (*C*) as previously described. Images and blots are representative of three separate experiments.

constructs. As shown in Fig. 6*A*, an intracellular FRET signal was observed, presumably in the ER and/or Golgi complex, with a weak signal observed at the plasma membrane. When quantified, co-expression of PAR$_2$ mEYFP and PAR$_4$ mECFP resulted in a significant increase in RFRET (1.883 ± 0.003) when compared with experimental conditions where collisional FRET could occur, *i.e.* co-expression of mEYFP and mECFP in cells yielded a RFRET value of 1.173 ± 0.055. Interaction between PAR$_2$ and PAR$_4$ was also demonstrated by co-immunoprecipitation in HEK293 cells as shown in Fig. 6*B*. These data indicate that PAR$_2$/PAR$_4$ heterodimerization occurs and is likely responsible for enhanced cell surface expression of PAR$_4$.

We then examined the role of PAR$_2$ in regulating further post-translational modification of PAR$_4$ in the context of receptor maturation and cell surface expression. *N*-Linked complex glycosylation is an important post-translational modification for efficient cell surface delivery of GPCRs (46). Analysis of the protein sequence of PAR$_4$ identified an Asn-Xxx-serine/threonine *N*-glycosylation motif located at position 56 (N^{56}DS) in the N terminus of the receptor (supplemental Fig. S1), suggesting that PAR$_4$ may undergo *N*-linked glycosylation. To assess this, first, pharmacological inhibition of glycosylation was carried out using the GlcNAc phosphotransferase inhibitor tunicamycin, which prevents all *N*-linked glycosylation. Fig. 7*A* shows that pretreatment of HEK293 cells with tunicamycin eliminated the higher molecular mass form of PAR$_4$, whereas the lower 65-kDa protein was still retained, with a minor intermediate band indicated. This effect was replicated in the R^{183}AR to A^{183}AA mutant, known to be preferentially expressed at the membrane. Experiments were then conducted using an N-terminal mutant of PAR$_4$ (Asn^{56} → Ala^{56}) to determine the effect of PAR$_2$ upon protein species expression (Fig. 7*B*) and receptor localization (Fig. 7*C*). In control NCTC cells the PAR$_4$ N^{56}A mutant construct (Fig. 7*B*, *top panel*) was expressed as a single 65-kDa protein form that corresponded to wild type PAR$_4$ mECFP. When expressed in NCTC-PAR$_2$ cells (Fig. 7*B*, *middle panel*) a loss in the higher molecular mass protein form was observed in comparison to wild type PAR$_4$ mECFP, however, the 65-kDa species was expressed alongside the slightly higher molecular mass form previously observed in the tunicamycin inhibition experiments. Similar results were obtained following expression in HEK293 cells (Fig. 7*B*, *lower panel*). Corresponding fluorescence microscopy images are shown in Fig. 7*C*. Lack of PAR$_4$ cell surface expression was observed following expression of the PAR$_4$ N^{56}A mutant in NCTC-PAR$_2$ cells.

Finally, the effect of enhanced cell surface expression of PAR$_4$ in the presence of PAR$_2$ was explored further in relationship to

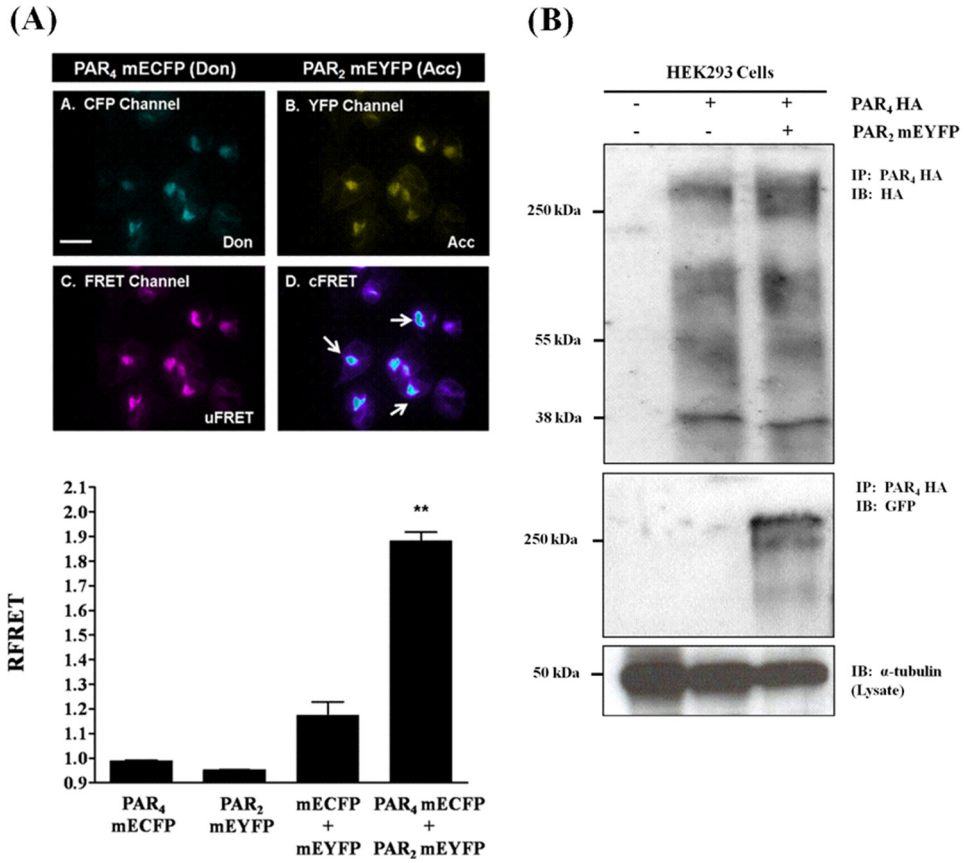

FIGURE 6. **FRET imaging and co-immunoprecipitation reveals heterodimer formation between PAR$_2$ and PAR$_4$ in HEK293 cells.** PAR$_4$ mECFP and PAR$_2$ mEYFP were co-expressed in HEK293 cells. Wide field FRET imaging was performed in live cells. *A*, images were acquired for CFP, YFP, uncorrected FRET (*uFRET*), with the uFRET channel corrected for spectral bleed-through/contamination (*cFRET*). *Scale bars* = 25 μm. Corresponding ratiometric FRET values were then quantified and graphed. Data are expressed as mean ± S.E. from three separate FRET experiments (n = 72 single cell measurements), **, p = 0.001 one-way analysis of variance with Dunnett's post-test. *B*, interaction between PAR$_4$-HA and PAR$_2$ mEYFP was further assessed by co-immunoprecipitation (*IP*). Blots are representative of at least three independent experiments.

PAR$_4$-mediated cell signal transduction. As shown in Fig. 8, NCTC-2544 and NCTC-PAR$_2$ cells transiently expressing PAR$_4$ mECFP produced an increase in basal inositol phosphate generation (NCTC, 4.59 ± 0.45; NCTC-PAR$_2$, 8.28 ± 0.65-fold of basal) compared with mock transfected cells. When each of these cell systems was treated with the PAR$_4$-specific activating peptide, AYPGKF-NH$_2$, a further increase in the inositol phosphate response was observed. When PAR$_4$ was expressed in NCTC-PAR$_2$ cells total inositol phosphate (InsP$_{1-4}$) accumulation (50 μM agonist; 22.47 ± 0.45 and 100 μM agonist; 21.16 ± 2.62-fold of basal) was substantially greater than observed following expression of PAR$_4$ in NCTC-2544 cells (50 μM agonist; 7.80 ± 0.46 and 100 μM agonist; 9.47 ± 2.45-fold of basal).

DISCUSSION

Receptor traffic from the ER to the plasma membrane involves highly coordinated events that in many cases may require numerous accessory proteins and motif-based sorting processes (35). The work presented here explores the mechanisms through which PAR$_4$ localization may be regulated. We demonstrate for the first time the fundamental structural properties and protein interactions that govern PAR$_4$ trafficking to the plasma membrane. Furthermore, we reveal the critical role of PAR$_2$ in aiding plasma membrane expression of PAR$_4$.

Initially we used bioinformatic analysis, which indicated that PAR$_4$ possesses a potential arginine-based (RXR) ER retention motif in intracellular loop 2, similar in sequence to those of the KA2 kainate (47) and 5HT$_{3B}$ serotonin (45) receptors. As such, we considered that this motif might be responsible for retention of PAR$_4$ in the ER as an immature protein as shown in Fig. 1. Unlike the KA2R and 5HT$_{3B}$R, however, where mutation of the motif did not affect ER retention, mutation of the R^{183}AR sequence of PAR$_4$ resulted in enhanced cell surface expression as assessed by both indirect immunofluorescence and subcellular fractionation. These findings are similar to previous studies showing efficient surface delivery following mutagenesis of a RSRR retention motif located within the C-terminal of the GABA$_{B1}$ polypeptide (24, 48). Protein complexes such as COPI can target other proteins for retention through recognition and interaction with RXR ER retention sequences (29), as demonstrated for retention of KA2 receptors (33) and, indeed, our studies showed PAR$_4$ interaction with the β-COP subunit of the COPI complex (Fig. 2*D*). Equally, ER retention of KA2R has been shown to correlate with an interaction with subunits that comprise the COPI chaperone system (33). Misfolded proteins or those containing sorting motifs such an ER retention motif are known to be shuttled back to the ER via COPI-containing vesicles (29). Our data in Fig. 4 show

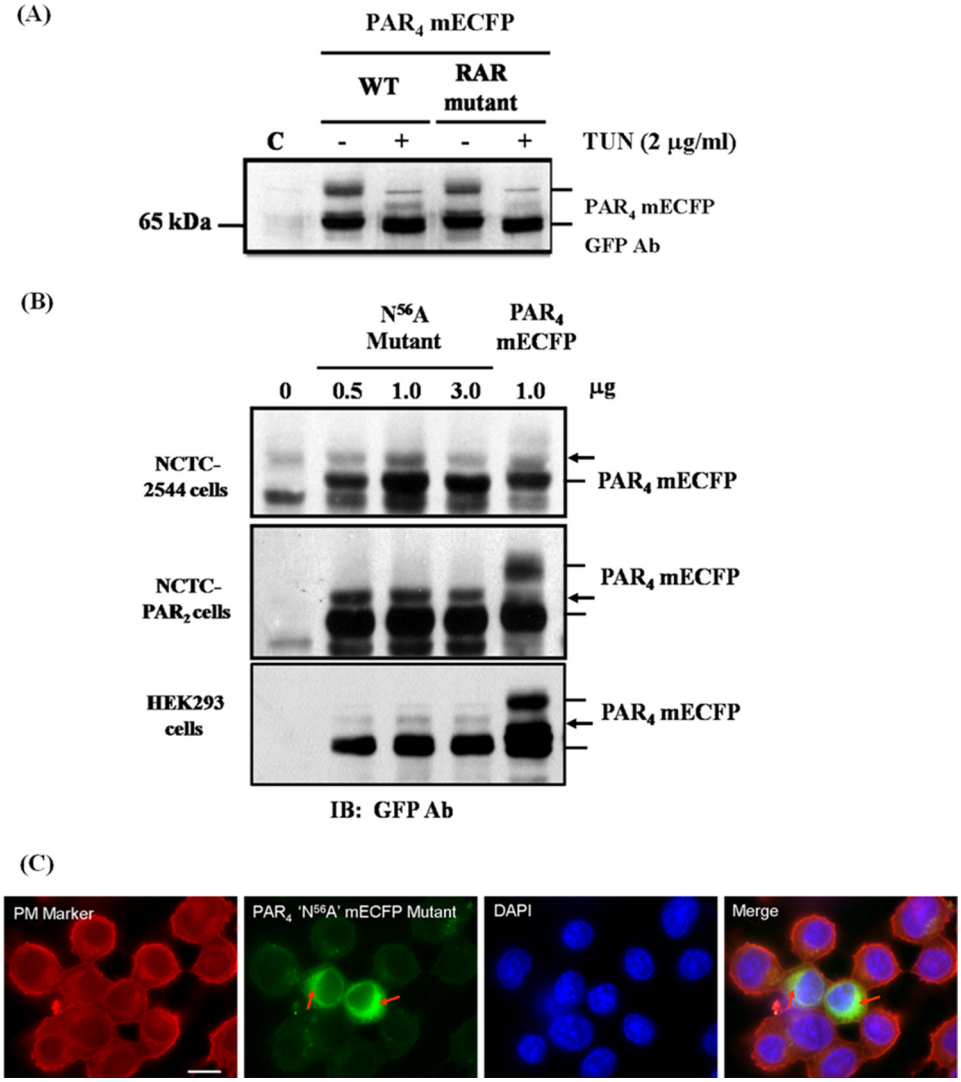

FIGURE 7. **The presence of PAR$_2$ allows *N*-linked glycosylation of PAR$_4$, which promotes membrane localization.** HEK293 cells were transfected with (*A*) PAR$_4$ mECFP or PAR$_4$ RAR mutant constructs. Prevention of *de novo N*-glycosylation was carried out by the addition of tunicamycin (2 μg/ml) to transfected cells as indicated for 16 h. *B,* NCTC, NCTC-PAR$_2$, and HEK293 cells were transfected with increasing concentrations of the PAR$_4$ N^{56}A mECFP mutant or PAR$_4$ mECFP. Whole cell lysates were prepared and resolved by Western blotting. *C,* fluorescent microscopy confirmed a loss of surface localization of PAR$_4$ following mutation of *N*-glycosylation site (*red arrows*). Cells were visualized using a ×100 Plan Fluor objective. *Scale bars* = 10 μm. Blots and images are representative of three independent experiments.

that indeed PAR$_4$ is retrieved via a COPI-mediated system, as found for KA2R.

Having defined the subcellular retention of PAR$_4$, we sought to determine what mechanisms might facilitate transport to the membrane because PAR$_4$ is able to signal in a number of cell types (49–51) and must reach the cell surface to be cleaved by the proteinase agonists. One potential candidate was PAR$_2$ because this receptor is often co-expressed with PAR$_4$ and has been shown to be co-activated by common agonists (20, 36, 37). However, a key issue in exploring this possibility was the fact that most cell lines currently studied express endogenous PAR$_2$ at some level. In this present study, characterization of PAR$_4$ subcellular distribution utilized NCTC-2544 cells because these express negligible PAR receptor levels and this allowed a direct assessment of the cellular distribution and function of PAR$_4$ in the absence and presence of PAR$_2$. Indeed, prior stable expression of PAR$_2$ in this cell line revealed enhanced PAR$_4$ plasma membrane expression compared with control NCTC cells. These results were recapitulated in HEK293 cells that are known to express endogenous PAR$_2$ and in other cells types we examined including human umbilical vein endothelial cells and PC3 cells (not shown), which are also known to express PAR$_2$ endogenously. Significantly, we show that enhanced plasma membrane delivery of PAR$_4$ by PAR$_2$ has functional sequelae, including increasing PAR$_4$-mediated inositol phosphate accumulation stimulated by a selective PAR$_4$ agonist. To our knowledge this is the first study to reveal such an interaction.

How may the presence of PAR$_2$ facilitate PAR$_4$ trafficking to the membrane? In the secretory pathway proper folding and assembly of GPCRs is essential for their efficient export to the cell membrane and function (52). Isoforms of 14-3-3 proteins have been shown to recognize and mask RXR motifs to direct ER/Golgi export of multimeric proteins (34, 53). Interestingly, we found that in the presence of PAR$_2$, PAR$_4$ becomes associated with 14-3-3ζ and at the same time loses its association with β-COP1. This competitive interaction is similar to that

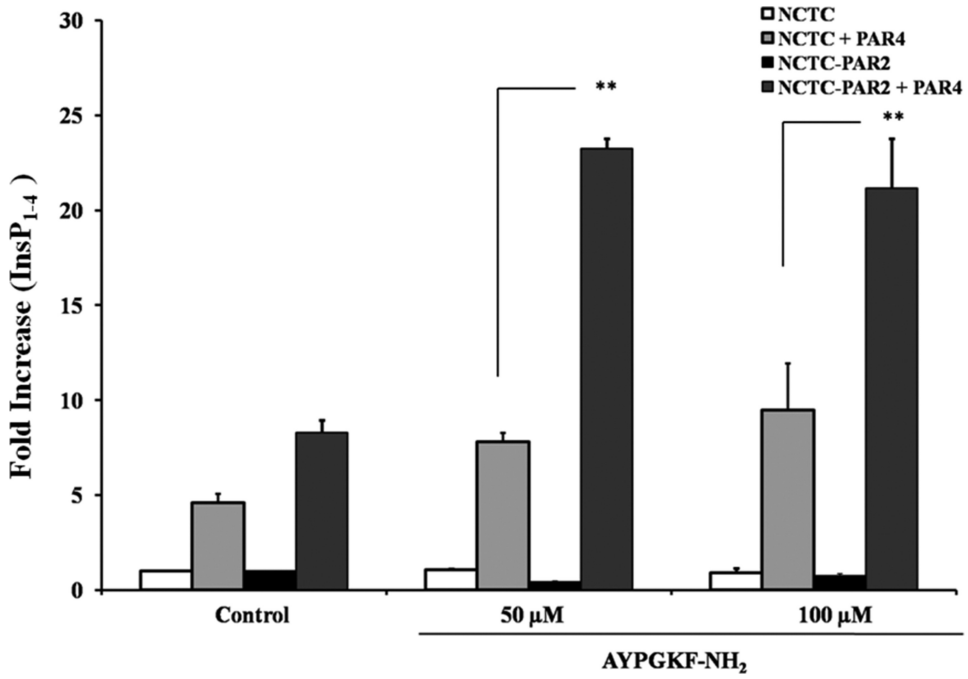

FIGURE 8. **Enhanced PAR$_4$-mediated [^{3}H]inositol phosphate accumulation in the presence of PAR$_2$.** NCTC-2544 and NCTC-PAR$_2$ cells transiently expressing PAR$_4$ mECFP were serum starved with serum-free growth medium supplemented with 0.25 μCi of *myo*-[2-^{3}H]inositol for 24 h. Cells were pretreated with 10 mM lithium chloride for 15 min prior to stimulation with AYPGKF-NH$_2$ as indicated for 45 min. Total inositol phosphate (InsP$_{1-4}$) accumulation was measured via anion exchange. The data are representative values performed in triplicate (mean ± S.E.) over three independent experiments (**, $p = <0.01$).

observed for an ATP-sensitive potassium (K_{ATP}) channel, in which COPI competes with 14-3-3ϵ and -ζ isoforms for interaction with the RKR motif on the cytosolic domain of each α subunit of the channel to facilitate ER retention (34). Because we also demonstrate PAR$_2$/PAR$_4$ heterodimerization by FRET and co-immunoprecipitation, this suggests that interaction with PAR$_2$ increases the affinity of PAR$_4$ for 14-3-3 binding. Thus, we have identified a critical early checkpoint in the secretory pathway involved in the processing of PAR$_4$ and PAR$_2$/PAR$_4$ heterodimer assembly, involving COPI and 14-3-3ζ chaperone systems, which explains the effects described above. Interestingly, when similar FRET experiments were conducted in the NCTC-2544 cell model, where co-expression with PAR$_2$ enhances surface expression with minimal intracellular compartmentalization, interaction at the membrane was negligible.[3] Unlike the ability of class C GPCRs to form stable dimers, the current findings may indicate interaction between PAR$_2$ and PAR$_4$ to be of a reversible and transient nature. This is akin to a number of other recent examples of GPCR dimerization that are transient and presumably defined by Mass-Action (54, 55). This would both allow PAR$_4$ to evade intracellular retention and, once at the cell surface, to be free to function in a monomeric or homodimeric state. This concept is currently under investigation.

We provided further confirmation of a role of PAR$_2$ in regulating PAR$_4$ trafficking in the context of *N*-linked glycosylation. This was initially detailed by pretreatment of wild type-PAR$_4$ (or the RAR mutant receptor) with tunicamycin or expression of PAR$_4$ mutated at the *N*-linked motif, located at position N^{56}DS within the N-terminal domain. Both approaches abolished the presence of the mature PAR$_4$ form and prevented cell surface expression. Similar effects have previously been shown for the dopamine D$_5$ receptor (46) where mutagenesis of specific Asn-linked motifs resulted in ER retention of the receptor. Despite the presence of an *N*-linked glycosylation motif (N^{56}DS), PAR$_4$ was unable to undergo complex glycosylation, unless in the presence of PAR$_2$. We also identified that *N*-glycosylation was a critical process in PAR$_2$-mediated delivery of PAR$_4$ to the cell surface. Mutagenesis of the *N*-linked motif resulted in intracellular retention of PAR$_4$, despite the presence of PAR$_2$.

To our knowledge, despite work detailing the involvement of COPI/14-3-3 in the intracellular transport of class C GPCRs and ion channels, our data are the first to describe such interactions for a well established class A GPCR family such as the PAR family. However, recent studies on the intracellular trafficking of a class A orphan GPCR, GPR15, detailed a critical role for the binding of 14-3-3 (to an RXR motif located at the extreme C-tail of the receptor) in its surface localization (56).

Although studies have demonstrated PAR$_1$/PAR$_4$ (57) and PAR$_1$/PAR$_3$ heterodimerization (58), this is the first study to reveal a functional interaction between PAR$_2$/PAR$_4$. Heterodimer formation between PAR$_2$ and PAR$_4$ impacted significantly upon other protein interactions with COPI and 14-3-3ζ, and by affecting the subcellular localization of PAR$_4$, substantially enhanced PAR$_4$-mediated signal transduction. PAR$_2$ and PAR$_4$ have been previously shown to be dual up-regulated by tumor necrosis factor α, a potent proinflammatory mediator (59, 60). An increase in PAR$_2$ has been linked to the progression of chronic inflammation (2, 61), with a role for PAR$_4$ in acute inflammation being implicated in other models of arthritis (62,

[3] M. R. Cunningham, J. D. Pediani, G. Milligan, and R. Plevin, unpublished observations.

63). Co-expression of these receptors in these pathophysiological environments, where tumor necrosis factor α is abundant, may be pivotal to the progression of a PAR$_2$/PAR$_4$-mediated proinflammatory response. In this study we identified a novel heterodimer partnership formed between PAR$_2$/PAR$_4$, which allows PAR$_4$ to bypass COPI-dependent retrograde transport and exit the ER to undergo post-translational modification to be delivered to the plasma membrane as a mature glycoprotein. These findings may be important in the understanding of the roles of each receptor in the context of inflammation.

REFERENCES

1. Russell, F. A., and McDougall, J. J. (2009) Proteinase-activated receptor (PAR) involvement in mediating arthritis pain and inflammation. *Inflamm. Res.* **58,** 119–126
2. McIntosh, K. A., Plevin, R., Ferrell, W. R., and Lockhart, J. C. (2007) The therapeutic potential of proteinase-activated receptors in arthritis. *Curr. Opin. Pharmacol.* **7,** 334–338
3. Macfarlane, S. R., Seatter, M. J., Kanke, T., Hunter, G. D., and Plevin, R. (2001) Proteinase-activated receptors. *Pharmacol. Rev.* **53,** 245–282
4. Vu, T. K., Hung, D. T., Wheaton, V. I., and Coughlin, S. R. (1991) Molecular cloning of a functional thrombin receptor reveals a novel proteolytic mechanism of receptor activation. *Cell* **64,** 1057–1068
5. Vu, T. K., Wheaton, V. I., Hung, D. T., Charo, I., and Coughlin, S. R. (1991) Domains specifying thrombin-receptor interaction. *Nature* **353,** 674–677
6. Bouton, M. C., Jandrot-Perrus, M., Moog, S., Cazenave, J. P., Guillin, M. C., and Lanza, F. (1995) Thrombin interaction with a recombinant N-terminal extracellular domain of the thrombin receptor in an acellular system. *Biochem. J.* **305**, 635–641
7. Ishii, K., Gerszten, R., Zheng, Y. W., Welsh, J. B., Turck, C. W., and Coughlin, S. R. (1995) Determinants of thrombin receptor cleavage. Receptor domains involved, specificity, and role of the P3 aspartate. *J. Biol. Chem.* **270,** 16435–16440
8. Hoxie, J. A., Ahuja, M., Belmonte, E., Pizarro, S., Parton, R., and Brass, L. F. (1993) Internalization and recycling of activated thrombin receptors. *J. Biol. Chem.* **268,** 13756–13763
9. Shapiro, M. J., Trejo, J., Zeng, D., and Coughlin, S. R. (1996) Role of the thrombin receptor's cytoplasmic tail in intracellular trafficking. Distinct determinants for agonist-triggered versus tonic internalization and intracellular localization. *J. Biol. Chem.* **271,** 32874–32880
10. Tiruppathi, C., Yan, W., Sandoval, R., Naqvi, T., Pronin, A. N., Benovic, J. L., and Malik, A. B. (2000) G protein-coupled receptor kinase-5 regulates thrombin-activated signaling in endothelial cells. *Proc. Natl. Acad. Sci. U.S.A.* **97,** 7440–7445
11. Paing, M. M., Stutts, A. B., Kohout, T. A., Lefkowitz, R. J., and Trejo, J. (2002) β-Arrestins regulate protease-activated receptor-1 desensitization but not internalization or Down-regulation. *J. Biol. Chem.* **277,** 1292–1300
12. Paing, M. M., Johnston, C. A., Siderovski, D. P., and Trejo, J. (2006) Clathrin adaptor AP2 regulates thrombin receptor constitutive internalization and endothelial cell resensitization. *Mol. Cell. Biol.* **26,** 3231–3242
13. Wolfe, B. L., and Trejo, J. (2007) Clathrin-dependent mechanisms of G protein-coupled receptor endocytosis. *Traffic* **8,** 462–470
14. Gandhi, P. S., Chen, Z., Appelbaum, E., Zapata, F., and Di Cera, E. (2011) Structural basis of thrombin-protease-activated receptor interactions. *IUBMB Life* **63,** 375–382
15. Böhm, S. K., Khitin, L. M., Grady, E. F., Aponte, G., Payan, D. G., and Bunnett, N. W. (1996) Mechanisms of desensitization and resensitization of proteinase-activated receptor-2. *J. Biol. Chem.* **271,** 22003–22016
16. Roosterman, D., Schmidlin, F., and Bunnett, N. (2003) Rab5a and rab11a mediate agonist-induced trafficking of protease-activated receptor 2. *Am. J. Physiol. Cell Physiol* **284,** C1319–1329
17. Stalheim, L., Ding, Y., Gullapalli, A., Paing, M. M., Wolfe, B. L., Morris, D. R., and Trejo, J. (2005) Multiple independent functions of arrestins in the regulation of protease-activated receptor-2 signaling and trafficking. *Mol. Pharmacol.* **67,** 78–87
18. Luo, W., Wang, Y., and Reiser, G. (2007) p24A, a type I transmembrane protein, controls ARF1-dependent resensitization of protease-activated receptor-2 by influence on receptor trafficking. *J. Biol. Chem.* **282,** 30246–30255
19. Luo, W., Wang, Y., and Reiser, G. (2011) Proteinase-activated receptors, nucleotide P2Y receptors, and μ-opioid receptor-1B are under the control of the type I transmembrane proteins p23 and p24A in post-Golgi trafficking. *J. Neurochem.* **117,** 71–81
20. Xu, W. F., Andersen, H., Whitmore, T. E., Presnell, S. R., Yee, D. P., Ching, A., Gilbert, T., Davie, E. W., and Foster, D. C. (1998) Cloning and characterization of human protease-activated receptor 4. *Proc. Natl. Acad. Sci. U.S.A.* **95,** 6642–6646
21. Kahn, M. L., Zheng, Y. W., Huang, W., Bigornia, V., Zeng, D., Moff, S., Farese, R. V., Jr., Tam, C., and Coughlin, S. R. (1998) A dual thrombin receptor system for platelet activation. *Nature* **394,** 690–694
22. Shapiro, M. J., Weiss, E. J., Faruqi, T. R., and Coughlin, S. R. (2000) Protease-activated receptors 1 and 4 are shut off with distinct kinetics after activation by thrombin. *J. Biol. Chem.* **275,** 25216–25221
23. Sabri, A., Guo, J., Elouardighi, H., Darrow, A. L., Andrade-Gordon, P., and Steinberg, S. F. (2003) Mechanisms of protease-activated receptor-4 actions in cardiomyocytes. Role of Src tyrosine kinase. *J. Biol. Chem.* **278,** 11714–11720
24. Gassmann, M., Haller, C., Stoll, Y., Abdel Aziz, S., Biermann, B., Mosbacher, J., Kaupmann, K., and Bettler, B. (2005) The RXR-type endoplasmic reticulum-retention/retrieval signal of GABAB1 requires distant spacing from the membrane to function. *Mol. Pharmacol.* **68,** 137–144
25. Michelsen, K., Yuan, H., and Schwappach, B. (2005) Hide and run. Arginine-based endoplasmic reticulum-sorting motifs in the assembly of heteromultimeric membrane proteins. *EMBO Rep.* **6,** 717–722
26. Barlowe, C. (2000) Traffic COPs of the early secretory pathway. *Traffic* **1,** 371–377
27. Barlowe, C., d'Enfert, C., and Schekman, R. (1993) Purification and characterization of SAR1p, a small GTP-binding protein required for transport vesicle formation from the endoplasmic reticulum. *J. Biol. Chem.* **268,** 873–879
28. Barlowe, C., Orci, L., Yeung, T., Hosobuchi, M., Hamamoto, S., Salama, N., Rexach, M. F., Ravazzola, M., Amherdt, M., and Schekman, R. (1994) COPII, a membrane coat formed by Sec proteins that drive vesicle budding from the endoplasmic reticulum. *Cell* **77,** 895–907
29. Aridor, M., Bannykh, S. I., Rowe, T., and Balch, W. E. (1995) Sequential coupling between COPII and COPI vesicle coats in endoplasmic reticulum to Golgi transport. *J. Cell Biol.* **131,** 875–893
30. Zerangue, N., Schwappach, B., Jan, Y. N., and Jan, L. Y. (1999) A new ER trafficking signal regulates the subunit stoichiometry of plasma membrane K(ATP) channels. *Neuron* **22,** 537–548
31. Margeta-Mitrovic, M., Jan, Y. N., and Jan, L. (2000) A trafficking checkpoint controls GABA(B) receptor heterodimerization. *Neuron* **27,** 97–106
32. Ren, Z., Riley, N. J., Garcia, E. P., Sanders, J. M., Swanson, G. T., and Marshall, J. (2003) Multiple trafficking signals regulate kainate receptor KA2 subunit surface expression. *J. Neurosci.* **23,** 6608–6616
33. Vivithanaporn, P., Yan, S., and Swanson, G. T. (2006) Intracellular trafficking of KA2 kainate receptors mediated by interactions with coatomer protein complex I (COPI) and 14-3-3 chaperone systems. *J. Biol. Chem.* **281,** 15475–15484
34. Yuan, H., Michelsen, K., and Schwappach, B. (2003) 14-3-3 dimers probe the assembly status of multimeric membrane proteins. *Curr. Biol.* **13,** 638–646
35. Duvernay, M. T., Filipeanu, C. M., and Wu, G. (2005) The regulatory mechanisms of export trafficking of G protein-coupled receptors. *Cell Signal.* **17,** 1457–1465
36. Sambrano, G. R., Huang, W., Faruqi, T., Mahrus, S., Craik, C., and Coughlin, S. R. (2000) Cathepsin G activates protease-activated receptor-4 in human platelets. *J. Biol. Chem.* **275,** 6819–6823
37. Cottrell, G. S., Amadesi, S., Grady, E. F., and Bunnett, N. W. (2004) Trypsin IV, a novel agonist of protease-activated receptors 2 and 4. *J. Biol. Chem.* **279,** 13532–13539
38. Zacharias, D. A., Violin, J. D., Newton, A. C., and Tsien, R. Y. (2002) Partitioning of lipid-modified monomeric GFPs into membrane microdo-

mains of live cells. *Science* **296,** 913–916
39. Plevin, R., Kellock, N. A., Wakelam, M. J., and Wadsworth, R. (1994) Regulation by hypoxia of endothelin-1-stimulated phospholipase D activity in sheep pulmonary artery cultured smooth muscle cells. *Br. J. Pharmacol.* **112,** 311–315
40. Proctor, K. M., Miller, S. C., Bryant, N. J., and Gould, G. W. (2006) Syntaxin 16 controls the intracellular sequestration of GLUT4 in 3T3-L1 adipocytes. *Biochem. Biophys. Res. Commun.* **347,** 433–438
41. Wilson, S., Wilkinson, G., and Milligan, G. (2005) The CXCR1 and CXCR2 receptors form constitutive homo- and heterodimers selectively and with equal apparent affinities. *J. Biol. Chem.* **280,** 28663–28674
42. Ellis, J., Pediani, J. D., Canals, M., Milasta, S., and Milligan, G. (2006) Orexin-1 receptor-cannabinoid CB1 receptor heterodimerization results in both ligand-dependent and -independent coordinated alterations of receptor localization and function. *J. Biol. Chem.* **281,** 38812–38824
43. Lopez-Gimenez, J. F., Canals, M., Pediani, J. D., and Milligan, G. (2007) The α_{1b}-adrenoceptor exists as a higher-order oligomer. Effective oligomerization is required for receptor maturation, surface delivery, and function. *Mol. Pharmacol.* **71,** 1015–1029
44. Kanke, T., Macfarlane, S. R., Seatter, M. J., Davenport, E., Paul, A., McKenzie, R. C., and Plevin, R. (2001) Proteinase-activated receptor-2-mediated activation of stress-activated protein kinases and inhibitory κB kinases in NCTC 2544 keratinocytes. *J. Biol. Chem.* **276,** 31657–31666
45. Boyd, G. W., Doward, A. I., Kirkness, E. F., Millar, N. S., and Connolly, C. N. (2003) Cell surface expression of 5-hydroxytryptamine type 3 receptors is controlled by an endoplasmic reticulum retention signal. *J. Biol. Chem.* **278,** 27681–27687
46. Karpa, K. D., Lidow, M. S., Pickering, M. T., Levenson, R., and Bergson, C. (1999) *N*-Linked glycosylation is required for plasma membrane localization of D5, but not D1, dopamine receptors in transfected mammalian cells. *Mol. Pharmacol.* **56,** 1071–1078
47. Nasu-Nishimura, Y., Hurtado, D., Braud, S., Tang, T. T., Isaac, J. T., and Roche, K. W. (2006) Identification of an endoplasmic reticulum-retention motif in an intracellular loop of the kainate receptor subunit KA2. *J. Neurosci.* **26,** 7014–7021
48. Pagano, A., Rovelli, G., Mosbacher, J., Lohmann, T., Duthey, B., Stauffer, D., Ristig, D., Schuler, V., Meigel, I., Lampert, C., Stein, T., Prezeau, L., Blahos, J., Pin, J., Froestl, W., Kuhn, R., Heid, J., Kaupmann, K., and Bettler, B. (2001) C-terminal interaction is essential for surface trafficking but not for heteromeric assembly of GABA(b) receptors. *J. Neurosci.* **21,** 1189–1202
49. Wu, C. C., Wu, S. Y., Liao, C. Y., Teng, C. M., Wu, Y. C., and Kuo, S. C. (2010) The roles and mechanisms of PAR4 and P2Y12/phosphatidylinositol 3-kinase pathway in maintaining thrombin-induced platelet aggregation. *Br. J. Pharmacol.* **161,** 643–658
50. Ando, S., Otani, H., Yagi, Y., Kawai, K., Araki, H., Fukuhara, S., and Inagaki, C. (2007) Proteinase-activated receptor 4 stimulation-induced epithelial-mesenchymal transition in alveolar epithelial cells. *Respir. Res.* **8,** 31
51. Hirano, K., Nomoto, N., Hirano, M., Momota, F., Hanada, A., and Kanaide, H. (2007) Distinct Ca^{2+} requirement for NO production between proteinase-activated receptor 1 and 4 (PAR1 and PAR4) in vascular endothelial cells. *J. Pharmacol. Exp. Ther.* **322,** 668–677
52. Lippincott-Schwartz, J., Roberts, T. H., and Hirschberg, K. (2000) Secretory protein trafficking and organelle dynamics in living cells. *Annu. Rev. Cell Dev. Biol.* **16,** 557–589
53. Shikano, S., Coblitz, B., Wu, M., and Li, M. (2006) 14–3-3 proteins. Regulation of endoplasmic reticulum localization and surface expression of membrane proteins. *Trends Cell Biol.* **16,** 370–375
54. Hern, J. A., Baig, A. H., Mashanov, G. I., Birdsall, B., Corrie, J. E., Lazareno, S., Molloy, J. E., and Birdsall, N. J. (2010) Formation and dissociation of M1 muscarinic receptor dimers seen by total internal reflection fluorescence imaging of single molecules. *Proc. Natl. Acad. Sci. U.S.A.* **107,** 2693–2698
55. Fonseca, J. M., and Lambert, N. A. (2009) Instability of a class a G protein-coupled receptor oligomer interface. *Mol. Pharmacol.* **75,** 1296–1299
56. Okamoto, Y., and Shikano, S. (2011) Phosphorylation-dependent C-terminal binding of 14-3-3 proteins promotes cell surface expression of HIV co-receptor GPR15. *J. Biol. Chem.* **286,** 7171–7181
57. Leger, A. J., Jacques, S. L., Badar, J., Kaneider, N. C., Derian, C. K., Andrade-Gordon, P., Covic, L., and Kuliopulos, A. (2006) Blocking the protease-activated receptor 1–4 heterodimer in platelet-mediated thrombosis. *Circulation* **113,** 1244–1254
58. McLaughlin, J. N., Patterson, M. M., and Malik, A. B. (2007) Protease-activated receptor-3 (PAR3) regulates PAR1 signaling by receptor dimerization. *Proc. Natl. Acad. Sci. U.S.A.* **104,** 5662–5667
59. Hamilton, J. R., Frauman, A. G., and Cocks, T. M. (2001) Increased expression of protease-activated receptor-2 (PAR2) and PAR4 in human coronary artery by inflammatory stimuli unveils endothelium-dependent relaxations to PAR2 and PAR4 agonists. *Circ. Res.* **89,** 92–98
60. Ritchie, E., Saka, M., Mackenzie, C., Drummond, R., Wheeler-Jones, C., Kanke, T., and Plevin, R. (2007) Cytokine up-regulation of proteinase-activated-receptors 2 and 4 expression mediated by p38 MAP kinase and inhibitory κB kinase β in human endothelial cells. *Br. J. Pharmacol.* **150,** 1044–1054
61. Ferrell, W. R., Lockhart, J. C., Kelso, E. B., Dunning, L., Plevin, R., Meek, S. E., Smith, A. J., Hunter, G. D., McLean, J. S., McGarry, F., Ramage, R., Jiang, L., Kanke, T., and Kawagoe, J. (2003) Essential role for proteinase-activated receptor-2 in arthritis. *J. Clin. Invest.* **111,** 35–41
62. McDougall, J. J., Zhang, C., Cellars, L., Joubert, E., Dixon, C. M., and Vergnolle, N. (2009) Triggering of proteinase-activated receptor 4 leads to joint pain and inflammation in mice. *Arthritis Rheum.* **60,** 728–737
63. Russell, F. A., Veldhoen, V. E., Tchitchkan, D., and McDougall, J. J. (2010) Proteinase-activated receptor-4 (PAR4) activation leads to sensitization of rat joint primary afferents via a bradykinin B2 receptor-dependent mechanism. *J. Neurophysiol.* **103,** 155–163